JACS
JOURNAL OF THE AMERICAN CHEMICAL SOCIETY
Article
Cite This: J. Am. Chem. Soc. 2019, 141, 18193−18203
pubs.acs.org/JACS

# First-Principles Characterization of the Elusive I Fluorescent State and the Structural Evolution of Retinal Protonated Schiff Base in Bacteriorhodopsin

Jimmy K. Yu,[†,‡,§] Ruibin Liang,[†,§] Fang Liu,[∥] and Todd J. Martínez*[,†,‡,§]

[†]Department of Chemistry and The PULSE Institute, Stanford University, Stanford, California 94305, United States
[‡]Biophysics Program, Stanford University, Stanford, California 94305, United States
[§]SLAC National Accelerator Laboratory, 2575 Sand Hill Road, Menlo Park, California 94025, United States
[∥]Department of Chemical Engineering, Massachusetts Institute of Technology, Cambridge, Massachusetts 02138, United States

Supporting Information

**ABSTRACT:** The conversion of light energy into work is essential to life on earth. Bacteriorhodopsin (bR), a light-activated proton pump in *Archae*, has served for many years as a model system for the study of this process in photoactive proteins. Upon absorption of a photon, its chromophore, the retinal protonated Schiff base (RPSB), isomerizes from its native all-*trans* form to a 13-*cis* form and pumps a proton out of the cell in a process that is coupled to eventual ATP synthesis. Despite numerous time-resolved spectroscopic studies over the years, the details of the photodynamics of bR on the excited state, particularly the characterization of the I fluorescent state, the time-resolved reaction mechanism, and the role of the counterion cluster of RPSB, remain uncertain. Here, we use ab initio multiple spawning (AIMS) with spin-restricted ensemble Kohn−Sham (REKS) theory to simulate the nonadiabatic dynamics of the ultrafast photoreaction in bR. The excited state dynamics can be partitioned into three distinct phases: (1) relaxation away from the Franck−Condon region dominated by changes in retinal bond length alternation, (2) dwell time on the excited state in the I fluorescent state featuring an untwisted, bond length inverted RPSB, and (3) rapid torsional evolution to the conical intersection after overcoming a small excited state barrier. We fully characterize the I fluorescent state and the excited state barrier that hinders direct evolution to the conical intersection following photoexcitation. We also find that photoisomerization is accompanied by weakening of the interaction between RPSB and its counterion cluster. However, in contradiction with a recent time-resolved X-ray experiment, hydrogen bond cleavage is not necessary to reproduce the observed photoisomerization dynamics.

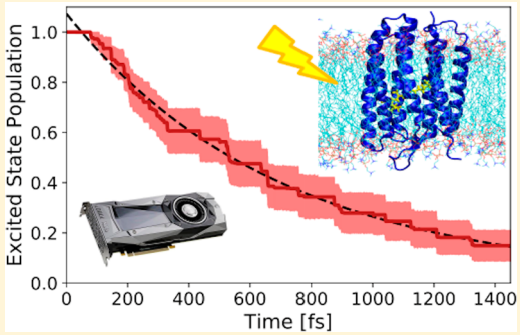




## INTRODUCTION

The ability to harness light as a usable form of biological energy is a fundamental component of life. Photoactive rhodopsin proteins, for example, participate in bioenergetic and homeostatic processes triggered by light.[1−3] In recent years, they have also found engineered applications as light-activated probes and optogenetic tools thanks to the ability to modulate the function of these proteins directly with light.[4] Bacteriorhodopsin (bR), a membrane protein discovered in *Halobacterium salinarum* almost 50 years ago,[1] has become a key example of a photoactive protein that triggers the bioenergetic cycle in *Archae*. Upon absorption of a photon, bR pumps a proton outward through the cell membrane to generate a proton gradient that is in turn coupled to the synthesis of ATP within the cell.[5,6] Due to the relative ease of working with bR experimentally and the early development of crystallization protocols for this membrane protein,[7] it has become a model system for the study for ultrafast photodynamics in biomolecules by a variety of spectroscopic and theoretical techniques.[8,9] The function of bR is modulated by its chromophore, the retinal protonated Schiff base (RPSB), which is covalently bound to the Lys216 residue by a Schiff base linkage (Figure 1a). In the ground state, RPSB in bR assumes an all-*trans* conformation when adapted to the presence of light. The absorption of a photon by bR triggers a highly efficient, specific, and rapid isomerization across the $C_{13}$═$C_{14}$ double bond of RPSB to produce a 13-*cis* photoproduct (Figure 1c).

Much of the interest in bR stems from the control of RPSB reactivity by the protein scaffolding, including a pentagonal counterion cluster, composed of three water molecules and the side chains of the Asp85 and Asp212 residues, that directly interacts with the Schiff base (Figure 1b). In methanol solvent, the RPSB has been observed to have an excited state lifetime on the order of 2−10 ps with a quantum yield of the 13-*cis* isomer around 0.05.[10,11] The double bond isomerization has also been observed to be nonspecific, as the 9-*cis* and 11-*cis*

Received: August 19, 2019
Published: October 17, 2019




DOI: 10.1021/jacs.9b08941
J. Am. Chem. Soc. 2019, 141, 18193−18203

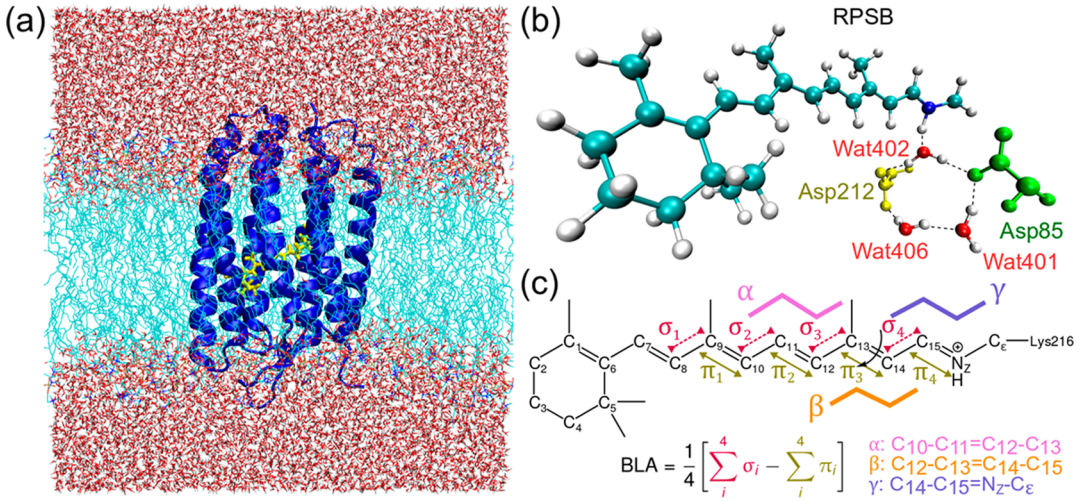


**Figure 1.** Details of our model for RPSB in bacteriorhodopsin (bR). (a) The RPSB chromophore (yellow licorice) is covalently bound to the chromophore pocket of the bR protein (blue ribbons). The protein, with the cytoplasmic side facing the top, is embedded in a POPC lipid bilayer (teal) and solvated by water (red). (b) The quantum mechanical region selected for the AIMD and AIMS simulations includes the entire RPSB chromophore plus $C_\epsilon H_2$ of the Lys216 side chain in addition to the pentagonal counterion cluster to the Schiff base, comprised of three water molecules (Wat401, Wat402, and Wat406) and the side chains of Asp85 and Asp212. (c) Schematic of the RPSB chromophore that indicates the naming convention used here. The ultrafast photoisomerization involves isomerization across the $C_{13}{=}C_{14}$ double bond, indicated by the black arrow. Three key dihedral angles are labeled $\alpha$, $\beta$, and $\gamma$, and the bond length alternation coordinate (BLA) is defined to be the total difference in single bond ($\sigma$) and double bond ($\pi$) lengths.

photoproducts are both formed in addition to the 13-*cis* photoproduct (see Figure 1c for the labeled RPSB) and dominate the overall photoproduct yield.[11] By contrast, in the protein, the photoisomerization of RPSB is extremely fast, decaying from the excited state within 500 fs,[12,13] highly efficient, isomerizing with a quantum yield above 0.6,[14,15] and specific, yielding only the 13-*cis* photoproduct or a recovery to the all-*trans* ground state following internal conversion.[16]

Despite several productive decades of work detailing the later parts of the bR photocycle,[8] the initial ultrafast photoreaction has been difficult to explicate to a comparable extent. The understanding of the excited state dynamics in bR has correlated strongly with advances in ultrafast spectroscopy in the last several decades. First, picosecond-resolution transient absorption experiments revealed the formation of the isomerized 13-*cis* intermediate K on the 3 ps time scale following photoexcitation.[17−19] The advent of femtosecond-resolution spectroscopy then allowed for the discovery of an even earlier isomerized intermediate J formed within 500 fs.[12,13,16,20,21] Research in the following decades has attempted to resolve further details of the excited state dynamics. Some of this work has suggested the possibility of a fluorescent excited state minimum structure (the I state), and the involvement of an excited state barrier between the Franck−Condon point and the conical intersection.[22−27] Transient absorption and stimulated emission experiments, however, are unable to provide the structural information necessary to resolve in detail the excited state evolution of RPSB and the photoisomerization mechanism, especially with respect to the behavior of the fluorescent excited state intermediate. This led to a shift toward the application of vibrational spectroscopy to femtosecond time scale investigations of photoactive proteins.[28−31] Recently, a methodological breakthrough in femtosecond serial X-ray crystallography has offered the ability to characterize intermediate structures during the ultrafast photoreaction by providing high resolution crystal structures of bR in the ground state, the excited state intermediate I, and the photoproduct states J and K, which have suggested that movement of the Schiff base counterion cluster may play an important role in the photoisomerization.[32,33]

Theory and simulation offer a unique opportunity to complement these experimental findings and probe aspects of the dynamics that experiments cannot: the reactive steps of the wavepacket on the excited state and the direct observation of the fluorescent excited state transient structure. Previous nonadiabatic dynamics studies on RPSB in bR have reported a barrierless decay of the excited state from the Franck−Condon region to the conical intersection, where internal conversion to the ground state occurs, within 200 fs.[9,34−37] These dynamics are inconsistent with experimental work that reports the existence of a fluorescent excited state intermediate in which the wavepacket becomes trapped on the excited state for a dwell time on the order of 500 fs.[24,28,38−41] Static studies have proposed an "aborted bicycle pedal" mechanism for the photoisomerization and speculated that a small (e.g., 1 kcal $mol^{-1}$) excited state barrier might lie between the Franck−Condon region and the conical intersection.[42,43] However, these studies could not provide dynamical observables to be compared to and/or validated by time-resolved experiments.

Three major pieces of the puzzle require further attention: (1) the time-resolved photoisomerization mechanism, (2) characterization of the elusive fluorescent excited state intermediate in the context of the nonadiabatic dynamics, and (3) elucidation of the role of the Schiff base counterions in the reactivity of RPSB in bR. Here, we study the ultrafast reactive step in a quantum mechanics/molecular mechanics (QM/MM) parametrization of the bR system using state-of-the-art nonadiabatic dynamics and electronic structure methods, *ab initio* multiple spawning (AIMS) dynamics with energies, forces, and nonadiabatic couplings from state-interaction state-averaged spin-restricted ensemble Kohn−Sham (SI-SA-REKS). Unlike previous simulations of retinal proteins, this combination simultaneously provides accurate descriptions of (1) quantum mechanics associated with


DOI: 10.1021/jacs.9b08941
J. Am. Chem. Soc. 2019, 141, 18193−18203

electronic surface crossings, (2) multireference character of electronic wave functions (static electron correlation) required for conical intersections, and (3) dynamic electron correlation effects known to have significant influence on the relative energies of conical intersections and excited state reaction paths. The resulting picture of the evolution of RPSB in bR following photoexcitation affirms the "aborted bicycle pedal" mechanism that Altoè et al. previously inferred from constrained energy minimizations with QM/MM methods.[43] Our simulations provide time-resolved spectra that we compare directly to previous spectroscopic measurements. The level of agreement obtained in these comparisons strongly suggests that the simulations are predictive, and we provide some evidence for this below. Because we simulate the excited state dynamics directly using an electronic structure method that includes dynamic correlation effects, we are able to address the dwell time and trapping of the fluorescent state on the excited state. We show that the fluorescent excited state intermediate features an untwisted, bond length inverted RPSB and quantify the small excited state barrier to be 3.4 kcal $mol^{-1}$. We also investigate the movement of the RPSB counterion cluster throughout the dynamics, which is compared directly to recent time-resolved X-ray diffraction experiments.

## THEORY AND METHODS

Our simulations start from the high-resolution crystal structure of bR (PDB ID: 6G7H)[32] obtained from time-resolved X-ray crystallography. Our simulation methodology includes the protein and surrounding membrane/solvent, and it has been recently validated for another RPSB-containing protein, channelrhodopsin 2.[44] The bR protein, including the RPSB chromophore and crystal waters, is embedded in a 1-palmitoyl-2-oleoyl-*sn*-glycero-3-phosphocholine (POPC) lipid bilayer and then solvated by water, as depicted in Figure 1a.[45,46] Because the RPSB chromophore is covalently bound to Lys216 side chain, we construct a special residue from the combined RPSB and Lys216 amino acid and generate a parametrization for it using the generalized Amber force field (GAFF).[47,48] The remainder of the protein is modeled by the Amber ff14SB force field,[49] the POPC lipids by the Amber Lipid14 force field,[50] and the waters by the SPC/Fw water model.[51] The protein is protonated according to the expected protonation state at neutral pH with the exceptions of Asp95, Asp115, Glu194, and Glu204, each of which is protonated according to previous experimental findings.[52,53]

The solvated, membrane-embedded bR system is first equilibrated using classical molecular dynamics with the OpenMM package.[54] The classical MD equilibration is performed in the NPT ensemble for 300 ns using 1 fs time steps, periodic boundary conditions (box dimensions of 90 Å × 90 Å × 95 Å), and the Langevin thermostat (300 K and 1 ps damping time) and Monte Carlo membrane barostat (1 atm) as implemented in OpenMM.[54,55] Thirty snapshots of the system are taken in time intervals of at least 1 ns from the final 50 ns of this equilibration trajectory. For each of these 30 snapshots, a subsystem containing the full bR protein and all lipids within a 5 Å radius and waters within a 10 Å radius of the protein is selected in order to reduce the computational expense of subsequent ab initio simulation steps (Figure S1). Each of these subsystems is then equilibrated for 2 ps using QM/MM in the NVT ensemble at 300 K with a time step of 0.5 fs. This QM/MM dynamics is performed using the GPU-accelerated TeraChem program with the Langevin thermostat (300 K and a 1 ps damping time).[56,57] The final coordinates and velocities from these QM/MM simulations are taken as initial conditions for AIMS dynamics starting on the $S_1$ excited state.

The QM/MM simulations (both ground state classical molecular dynamics and subsequent AIMS dynamics) use TeraChem for the QM region and OpenMM for the MM region.[54,58,59] The QM region consists of the full RPSB chromophore, the $C_\epsilon H_2$ unit from the Lys216 side chain, and the counterion cluster to the Schiff base, which includes three water molecules (Wat401, Wat402, and Wat406) and the side chains of Asp85 and Asp212 (74 atoms in total; Figure 1b). The remainder of the protein, the lipids, and the solvating waters are described using molecular mechanics with the same force fields as in the classical MD equilibration.

The QM region is described at the SI-SA-REKS level of theory using the range-corrected hybrid functional $\omega$PBEh ($\omega$ = 0.2) and the 6-31G basis set.[60−63] An active space of two active electrons in two orbitals, denoted (2,2), is chosen as appropriate for describing the $\pi \rightarrow \pi^*$ excitation character of RPSB.[44] The SI-SA-REKS(2,2) method is conceptually similar to the more conventional state-averaged complete active space self-consistent field (SA-CASSCF) method;[64] however, REKS employs an ensemble density functional theory (DFT) approach in order to account for multiple configurations, thus describing both dynamic and static electron correlation effects. In contrast to most variants of time-dependent density functional theory,[65] the SI-SA-REKS electronic structure method provides an accurate representation of conical intersections and regions of strong nonadiabatic coupling between potential energy surfaces as a result of its multiconfigurational character. It has previously been shown to accurately describe the geometries and energetics of minimal energy conical intersections for a variety of organic molecules,[66] including analogues of RPSB.[67] Moreover, dynamic correlation effects have been shown to be similarly important in the description of chromophores such as RPSB that feature a long conjugated chain.[68] The ability to describe both facets of electron correlation is enough to improve the behavior of SI-SA-REKS(2,2) relative to more conventional complete active space methods, thus making it a well-suited electronic structure method for studying RPSB.[44]

AIMS simulations are performed using the FMS90 dynamics program interfaced with TeraChem and OpenMM.[54,56,69−71] AIMS is a nonadiabatic dynamics method designed to simulate systems that require a description of multiple electronic states and is thus appropriate for a photochemical system like RPSB in bR. AIMS treats the nuclei as a quantum wavepacket and thereby includes quantum effects that are missing in trajectory surface hopping.[72−74] Given an initial condition of starting positions and momenta for the system, one trajectory basis function (TBF), a frozen Gaussian wavepacket, is placed on the excited state, i.e., vertically excited, and propagated classically with forces and nonadiabatic couplings computed directly with ab initio REKS-QM/MM. New TBFs are spawned on the ground state in regions of high nonadiabatic coupling, and population is transferred between the electronic states while the TBFs remain coupled in these regions. The newly spawned TBFs soon separate and continue to evolve independently upon leaving the coupling region, thus naturally accounting for the decoherence of the nuclear wave function over time. A consequence of the spawning procedure to describe the nonadiabatic transition between electronic states is the rapid convergence of the photoreaction branching ratio. Here, we select 30 initial conditions for AIMS dynamics from the QM/MM equilibration, as described above. The AIMS simulations are performed for up to 1.5 ps or until more than 95% of the excited state population has decayed to the ground state and the excited and ground state dynamics are fully decoupled. The results of the 30 AIMS simulations are averaged in order to study the isomerization mechanism and the excited state dynamics. The MDTraj software package is used in our analysis of relevant dihedral angles and bond lengths.[75]

## RESULTS

**Validation of Electronic Structure and Nonadiabatic Dynamics.** One of the difficulties, both experimentally and theoretically, in fully characterizing the ultrafast photoreaction of RPSB in bR has been the time-resolution of the individual stages of the reaction. We approach this first by examining the decay of the excited state. The population decay of the excited state and its complementary recovery on the ground state are


DOI: 10.1021/jacs.9b08941
J. Am. Chem. Soc. 2019, 141, 18193−18203

computed for the nonadiabatic dynamics averaged over the 30 AIMS simulations and reported in Figure 2. By the end of our

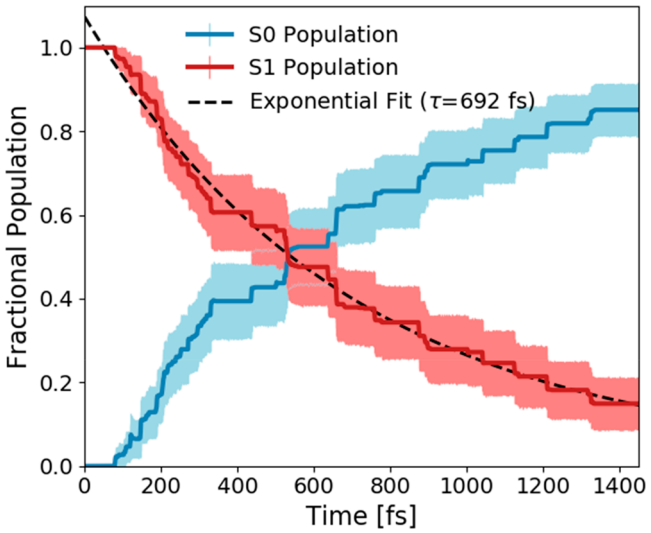


**Figure 2.** Decay of the excited state population and the rise of ground state population (solid curves) from the AIMS simulations of photoexcited bR is plotted here with error bars representing one standard error computed by bootstrapping. A single exponential function (dashed curve) is used to fit the decay and yields a time constant $\tau$ = 692 ± 221 fs.

simulations, at 1450 fs, 85% of the excited state population has decayed to the ground state. The stepped decay pattern in the averaged population decay is a result of the extremely fast and efficient internal conversion step (to be discussed shortly) and may also indicate a specific promoting vibrational mode that governs access to the conical intersection on the excited state (Figure S2). The time evolution of the $S_1$ excited state population is fit using a single exponential function and yields an estimate of $\tau$ = 692 ± 221 fs for the excited state lifetime. Numerous spectroscopic experiments during the past four decades have reported a consensus of $\tau \approx 500$ fs for the excited state lifetime and the photoproduct formation time scale.[12,13,25,31,38,41] The excited state lifetime measured in our simulation is thus consistent within experimental uncertainty.

In order to compare directly with experimental results (the direct population decay cannot be measured experimentally), we compute the time- and energy-resolved 2D fluorescence spectrum averaged over all 30 AIMS simulations as

$$I(t,\nu) \propto \sum_{I\in S_1} n_I(t)|\mu^I_{S_0S_1}(t)|^2\left(\frac{E^I_{S_1}(t) - E^I_{S_0}(t)}{h}\right)^3$$

where the sum is over all TBFs, enumerated by $I$, on the excited state. At each time point $t$, for the $I$th TBF, $n_I(t)$ is the excited state population, $\mu^I_{S_0S_1}$ is the transition dipole between the excited and ground state, and $E^I_{S_0/S_1}$ is the electronic energy on the excited or ground state, respectively. The simulated time/energy-resolved fluorescence spectrum features two dominating signals, one marking the Franck−Condon region in the short wavelength region (centered at ∼460 nm) and a second one at a longer wavelength (centered at ∼680 nm) (Figure 3a). The two gray horizontal lines in Figure 3a at 603 and 730 nm sandwich an energy region of our simulated fluorescence spectrum that has been probed by femtosecond fluorescence experiments.[41] The simulated fluorescence signal is red-shifted by 0.15 eV in order to match the single wavelength fluorescence traces at 603 and 730 nm in the simulation to experimental traces at 650 and 800 nm, all four of which are shown in Figure 3b. The value of this red shift is chosen by matching the maximal fluorescence wavelength in the time-integrated fluorescence signals (Figure S3). The rise, early decay, and tail of the fluorescence signals are in agreement between experiment and theory, while the nonexponential decay at intermediate times is within error of the experimental result. A key experimental observation, the wavelength-dependent behavior of the fluorescence spectrum, is reproduced in our simulations: the fluorescence maximum is attained later, and the excited state decay is slower for single wavelength traces at longer wavelengths (Figures 3b and S4). The agreement between simulation and experiment thus provides confidence that the following discussion regarding the characterization of the fluorescent state and the time-resolved reactive mechanism based on our simulations reflects

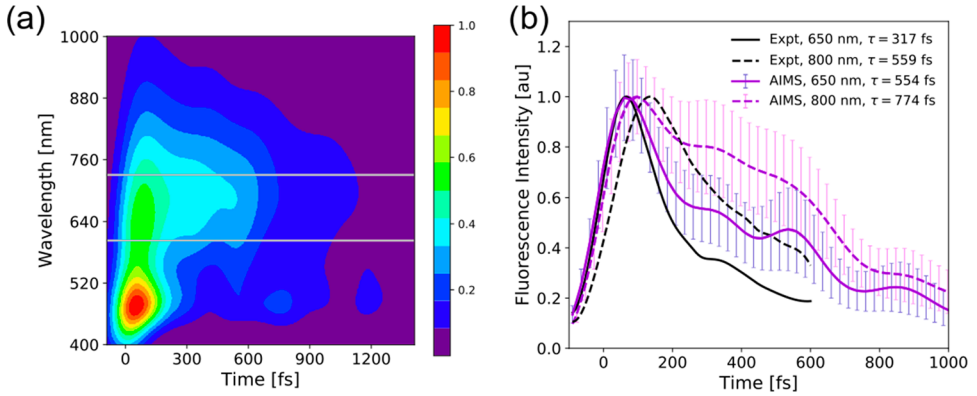


**Figure 3.** (a) 2D fluorescence spectrum computed from 30 AIMS simulations starting on the excited state with coloring scale indicated on the right. The two gray horizontal lines across the 2D fluorescence spectrum mark the wavelengths 603 and 730 nm that correspond to single wavelength fluorescence traces in (b). (b) Experimental fluorescence traces at 650 nm (solid) and 800 nm (dashed) are plotted in black,[41] and the corresponding fluorescence traces from simulation at 650 and 800 nm are plotted in purple. The simulated fluorescence signals have been red-shifted by 0.15 eV (603 and 730 nm unshifted) to match the time-integrated fluorescence maximum (see Figure S3). The error bars for the fluorescence traces, computed by bootstrapping, represent one standard error.



DOI: 10.1021/jacs.9b08941
J. Am. Chem. Soc. 2019, 141, 18193−18203

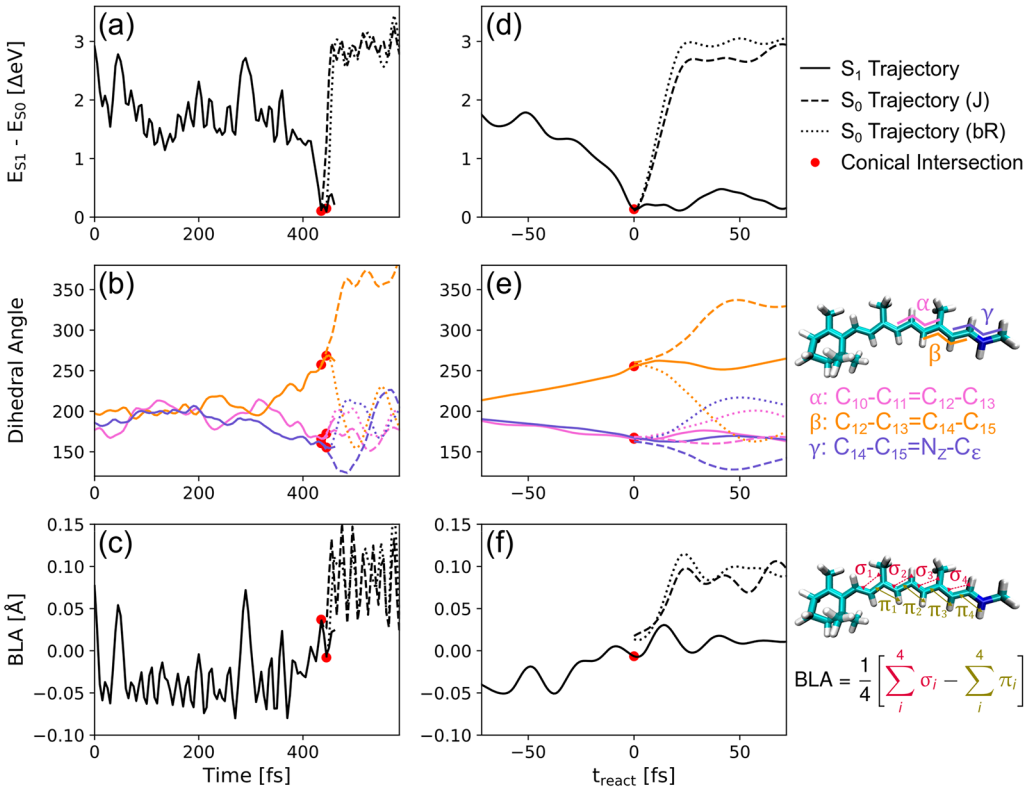


**Figure 4.** (a–c) Dynamics trace in time for a single representative AIMS simulation. In each trace, the solid line indicates the initial TBF propagating on the excited state, the dashed line indicates a TBF propagating on the ground state to form the 13-*cis* photoproduct (J), and the dotted line indicates the TBF propagating on the ground state to recover the all-*trans* reactant (bR). The red dot indicates the point of spawning (conical intersection), where significant nonadiabatic coupling causes population transfer and spawning of new TBFs on the ground state. Panel (a) traces the energy gap between the excited state and the ground state. Panel (b) traces three relevant dihedral angles labeled by color according to the legend on the right. $\alpha$ in purple tracks the $C_{10}$-$C_{11}$=$C_{12}$–$C_{13}$ dihedral angle, $\beta$ in orange tracks $C_{12}$–$C_{13}$=$C_{14}$–$C_{15}$, and $\gamma$ in blue tracks $C_{14}$–$C_{15}$=$N_Z$–$C_\varepsilon$. Panel (c) traces the evolution of the bond length alternation coordinate during the dynamics. (d–f) Dynamics trace on a reactive time scale and averaged over all AIMS simulations. The reactive time scale is defined here to be a 140 fs window of the dynamics centered at the first spawning point marked by the red circle. Panels (d)–(f) track the energy gap, dihedral angles, and bond length alternation coordinate, as in (a)–(c).

the true dynamics of RPSB in bR were they to be probed experimentally.

**The Bond Length Inverted Fluorescent State and the Excited State Barrier.** One of the outstanding questions in the study of the ultrafast photoreaction in bR involves the existence and characterization of the I fluorescent state and the possibility of a barrier between the fluorescent region of the excited state potential energy surface and the conical intersection. The fluorescent state has been suggested to be an excited state transient species and is thus difficult to characterize structurally, although it is a key component to popular experimental models.[8,25,26,76] Until recently, it was believed that the photoisomerization was a barrierless reaction,[12,13,27] which would preclude the existence of a long-lived fluorescent state. However, locked RPSB (preventing isomerization) studies have identified a possibly stable fluorescent state in the photocycle prior to the torsional motion associated with internal conversion to the ground state,[24,39,40] and some theoretical and experimental work has since suggested that a small excited state barrier may lie between the fluorescent state and the conical intersection.[42,43,77] Nonadiabatic dynamics studies of RPSB in bR until now have failed to identify such a fluorescent state for reasons possibly including truncations of the RPSB chromophore in the QM region, the omission of the counterion cluster from the QM region (see Figure S5), and inadequate descriptions of static and/or dynamic electron correlation. They have instead reported dynamics suggestive of ultrafast barrierless decay of the excited state on the time scale of $\tau \approx$ 200 fs.[34–36]

Our simulated time-resolved fluorescence spectrum in Figure 3a reveals a relatively long-lived (over 500 fs) fluorescent state in the 600–800 nm wavelength region in which the wavepacket population can be trapped on the excited state potential energy surface. By studying the photoisomerization mechanism with high time resolution in our simulations (see Figure 4), we have characterized the structure of RPSB in bR in this state. In the fluorescent region, RPSB is inverted in the bond length alternation (BLA) coordinate (defined in Figure 1c to be the average difference in the single and double bond lengths along the RPSB polyene chain) and is largely untwisted along the polyene chain, thus remaining in the all-*trans* conformation. RPSB samples small magnitude variations in the dihedral angles and vibrations along the polyene chain during the dwell time until it escapes from the fluorescent region and evolves rapidly to the conical intersection. Here, we have assigned the lower energy fluorescence signal in Figure 3a to be the fluorescent state.


DOI: 10.1021/jacs.9b08941
J. Am. Chem. Soc. 2019, 141, 18193–18203

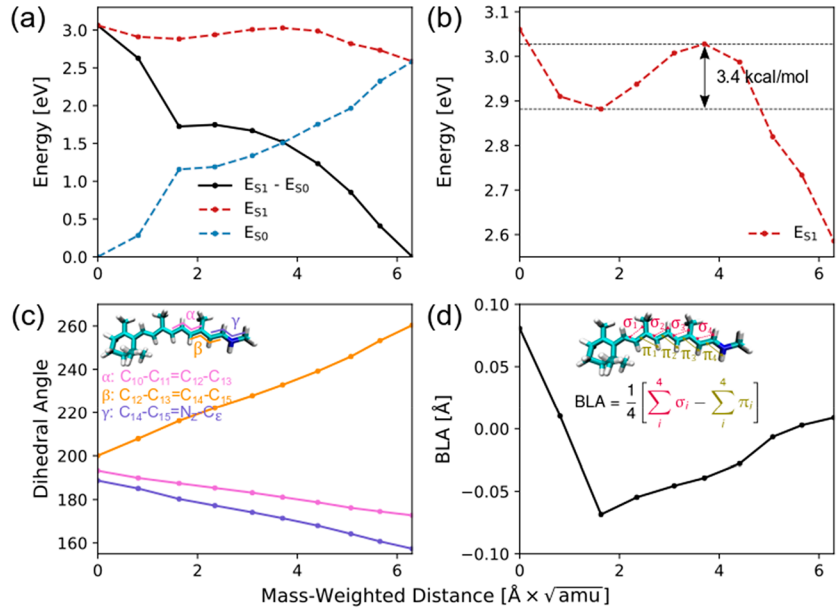


**Figure 5.** Minimum energy path from the ground state minimum geometry (bR) to the minimum energy conical intersection corresponding to the twisted RPSB (CI). The beads along the minimum energy path are marked as circles along the curves, and the energies/coordinates are plotted as functions of the mass-weighted distance along the reaction path. (a) The excited state energy is represented by a dashed red curve, the ground state energy by a dashed blue curve, and the $S_1$−$S_0$ energy gap by a solid black curve. (b) A zoomed-in plot of the excited state energy curve highlights the barrier on the excited state, computed here to be 3.4 kcal mol$^{-1}$. (c) The evolution of the three relevant dihedral angles along the minimum energy path. The color scheme is given in the inset showing the dihedral angles. (d) Evolution of the bond length alternation (BLA) coordinate along the minimum energy path. The inset provides the definition of the BLA coordinate measured here.

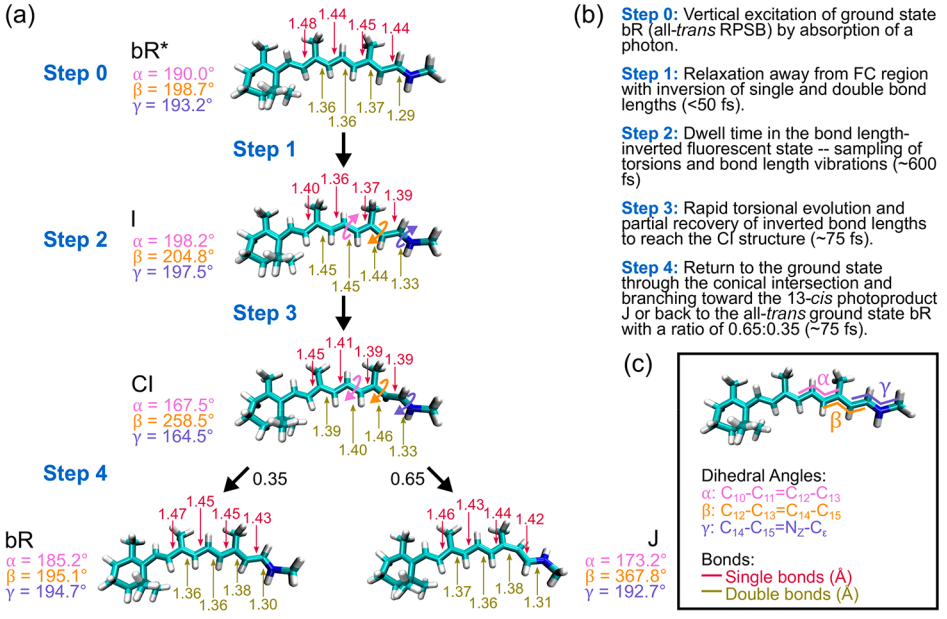


**Figure 6.** (a) Graphic depiction of the mechanism for the ultrafast reactive step with details of the key steps of the reaction mechanism described in (b) and a legend for the color scheme and labels used for the diagram in (c).

Although there is an initial burst of fluorescence in the Franck−Condon region around the absorption wavelength, it is extremely short-lived and would thus be difficult to observe spectroscopically.[41] Moreover, it does not correspond to the inverted BLA structure that gives rise to the delayed internal conversion of RPSB in bR. These dynamics involve a trapped fluorescent region that blocks the ballistic evolution of the wavepacket from the Franck−Condon region directly to the conical intersection and thus suggest a barrier on the excited state, with the subpicosecond lifetime of the excited state suggesting that the barrier height is small in magnitude.

In order to quantitatively characterize the excited state barrier, a static reaction path from the Franck−Condon region to the $C_{13}$═$C_{14}$-twisted conical intersection is computed at the SI-SA-REKS(2,2) level of theory (the same as that used for the nonadiabatic dynamics). The reaction path is shown in three relevant coordinates in Figure 5a, c, and d. Figure 5a tracks the excited state and ground state energies and the $S_1$−$S_0$ energy


DOI: 10.1021/jacs.9b08941
J. Am. Chem. Soc. 2019, 141, 18193−18203

gap along the reaction path. Figure 5b provides a zoomed-in view of the excited state energy along the reaction, where the wavepacket can be observed to access a local minimum at which the energy gap is ∼1.7 eV (Figure 5a), the magnitude of twisting in the three relevant dihedral angles $\alpha$, $\beta$, and $\gamma$ is small (Figure 5c), and the BLA coordinate is at a minimum (Figure 5d). Thus, at the local minimum in the $S_1$ state, the RPSB remains almost planar but the single and double bonds have inverted. This bond length inverted minimum is consistent with the I fluorescent state identified in our nonadiabatic dynamics simulations. In order to reach the conical intersection, the wavepacket must overcome a small 0.15 eV, or 3.4 kcal $mol^{-1}$, barrier. In the context of the simulated dynamics, the majority of the excited state lifetime is spent in the fluorescent region sampling configurations similar to the bond length inverted minimum here, accounting for roughly 600 fs of the excited state lifetime, whereas the other points on the reaction path before and after the fluorescent minimum are traversed within 100 fs collectively.

Our theoretical studies here thus help to characterize the elusive excited state transient I as an untwisted, bond length inverted structure in the fluorescent region of the excited state potential energy surface, and identify a small barrier that briefly traps the wavepacket on the excited state prior to internal conversion to the ground state. Having characterized this key stage of the excited state dynamics, we continue to deduce a step-by-step picture of the time-resolved photoisomerization mechanism informed by our simulations in the following.

**Three Stage Evolution on the Excited State Potential Energy Surface.** Distinct stages of the excited state evolution are visible in the time-resolved fluorescence spectrum (Figure 3a) and in traces of dynamic modes of the wavepacket in time (Figure 4). The mechanism described in the following is drawn visually in Figure 6.

The initial excitation of the bR system in the Franck−Condon region results in an intense but short-lived fluorescence signal at short wavelengths. The first stage of the evolution on the excited state potential energy surface is a rapid (<50 fs) movement of the wavepacket away from the Franck−Condon region to a longer-lived fluorescent region centered around 680 nm. This manifests as a smearing of the fluorescence signal between the Franck−Condon region and the fluorescent region in Figure 3a and a corresponding decrease in the $S_1$−$S_0$ energy gap from ∼3.0 to ∼1.7 eV in Figure 4a. Structurally, this process is associated with relaxation in the RPSB in the BLA coordinate (Figure S6). On the ground state and immediately after photoexcitation (at the Franck−Condon point), the single bonds are longer than the double bonds. As the wavepacket relaxes quickly into the fluorescent region, the double bonds elongate and the single bonds shorten, resulting in an inversion of the bond length alternation coordinate, as seen in "Step 1" of Figure 6a. This produces the bond length inverted fluorescent state characterized in the previous section.

The second stage of the excited state evolution involves the trapping of the wavepacket in the fluorescent region, visualized as "Step 2" of Figure 6a. This is visualized in Figure 3a as the longer-lived (∼600 fs lifetime) fluorescence signal between 600 and 800 nm. Mechanistically, this corresponds to the sampling of small magnitude variations in the torsional coordinates (Figure 4b) and vibrational sampling in the bond length alternation coordinate (Figure 4c). In this stage of the excited state dynamics, the RPSB chromophore mostly remains in the all-*trans* configuration and in its bond length inverted form. The dwell time in this fluorescent region is variable for each excited state trajectory but on the order of 500−700 fs and accounts for most of the time the wavepacket spends on the excited state.

The third and final stage of the excited state dynamics is the escape from the trapped fluorescent region and the rapid evolution to the conical intersection, where internal conversion to the ground state occurs. This stage is marked as "Step 3" in Figure 6a. The evolution to the conical intersection is marked visually by the smearing of the fluorescence signal toward long wavelengths: as the $E_{S_1}$−$E_{S_0}$ energy gap approaches zero, the corresponding fluorescence wavelength approaches infinity and the intensity also approaches zero. In this stage of the dynamics, the photoisomerization begins, marked by a unidirectional clockwise twist in the $\beta$ dihedral angle ($C_{12}$−$C_{13}$=$C_{14}$−$C_{15}$) from its pretwisted ∼200° native form to ∼270°, characteristic of the conical intersection geometry (Figure S7). The clockwise motion in the $\beta$ dihedral angle is accompanied by smaller magnitude twists in the opposite direction for the $\alpha$ and $\gamma$ dihedral angles ($C_{10}$−$C_{11}$=$C_{12}$−$C_{13}$ and $C_{14}$−$C_{15}$=$N_Z$−$C_\varepsilon$, respectively) in order to preserve space in the chromophore pocket and compensate for the torsion in $\beta$ (Figure S8). This coincides with a recovery of the inversion in the bond length alternation coordinate to a neutral state. This third stage of the excited state dynamics culminates in internal conversion as the wavepacket accesses the twisted conical intersection, indicated by the red dots in Figure 4.

Upon internal conversion to the ground state, the ultrafast photoreaction rapidly approaches completion. From the conical intersection, the RPSB either reverts to the all-*trans* conformation, thus recovering the ground state (bR) or the reaction proceeds to completion, resulting in the 13-*cis* photoproduct (J), as pictured as "Step 4" in Figure 6a. The recovered ground state and isomerized photoproduct are produced in a 0.35:0.65 ratio, consistent with experimental work reporting a 65% quantum yield for the photoreaction.[14,15] The torsional motion accounts for only a small time window of the photoreaction, as demonstrated in Figure 4d−f, which shows the average of the 30 AIMS simulations within a 140 fs time window centered at the first spawning point, the first time the excited state trajectory encounters the conical intersection. On the excited state, the simultaneous narrowing of the $E_{S_1}$−$E_{S_0}$ energy gap, torsional motion, and recovery in the bond length alternation coordinate occur within this small 70 fs time window for all trajectories. Formation of the photoproducts (recovery of bR or isomerization to J) and completion of the torsional motion of the photoreaction occurs similarly quickly, within 50 fs after internal conversion.

In trajectories that complete the photoisomerization, the "aborted bicycle pedal" mechanism, previously hypothesized in static theoretical studies,[43] can be seen, marked by the counterclockwise twisting of the $\alpha$ and $\gamma$ dihedral angles to compensate for the clockwise twisting of $\beta$ on the excited state and then recovery in $\alpha$ and $\gamma$ as $\beta$ rotates to completion on the ground state. For the first time, we can assign a time scale to the "aborted bicycle pedal" portion of the full photoreaction. As observed in Figure 4e, the primary torsion in the reaction proceeds from start to finish in this small time window of 70 fs before plus 50 fs after internal conversion, accounting for only ∼120 fs of the ∼750 fs (692 fs on the excited state and ∼50 fs on the ground state) required to fully isomerize following


DOI: 10.1021/jacs.9b08941
J. Am. Chem. Soc. 2019, 141, 18193−18203

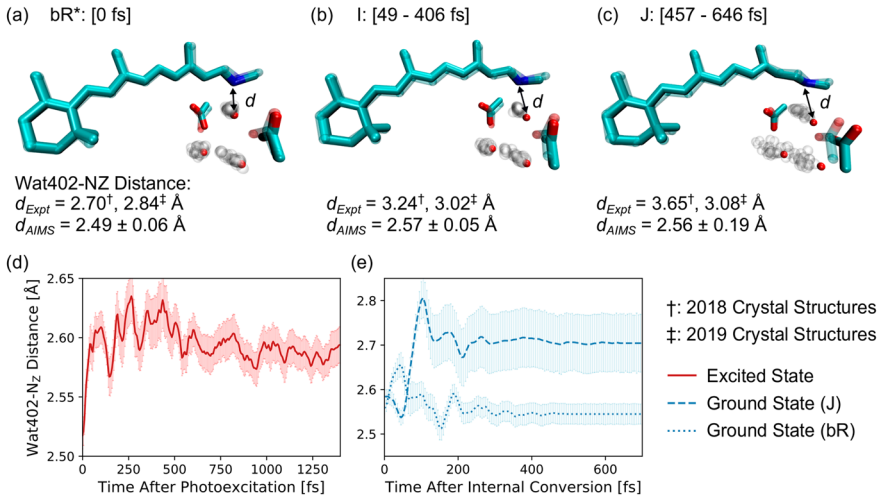


**Figure 7.** Comparison between experimental crystal structures and our simulation results at three critical points: (a) the Franck−Condon point (bR*), (b) the I fluorescent state, and (c) the isomerized photoproduct J. The RPSB and the pentagonal counterion cluster from the experimental crystal structures (PDB accession codes: 6G7H, 6G7I, and 6G7J)[32] are visualized in the opaque licorice representation, and the corresponding molecular structures from our AIMS simulations are shown in the transparent licorice representation. The simulated bR*, I, and J structures are taken as averages over all 30 AIMS simulations in time windows corresponding to the time windows described by the crystal structures: 0 fs for bR*, 49−406 fs for I, and 457−646 fs for J. The average positions of the three water molecule oxygens in each of the 30 AIMS simulations are visualized as transparent gray spheres in order to show their spatial distribution in our simulated structures relative to the positions of the three waters in the crystal structures (opaque red sphere). The Wat402−$N_Z$ distance, labeled by a black double-headed arrow, is reported for the 2018 crystal structures (†), the recently published 2019 crystal structures (‡), and our simulations for comparison. The average Wat402−$N_Z$ distance is tracked in (d) while the wavepacket is on the excited state after photoexcitation (red) and in (e) following internal conversion to the ground state for the 13-*cis* photoproduct J (dashed blue) and the recovered ground state bR (dotted blue). The error bars for the average Wat402−$N_Z$ distance, obtained from bootstrapping, represent one standard error.

photoexcitation. Now that we have outlined the distinct phases of the reaction dynamics, we turn to a closer examination of the critical structures and intermediates in our simulations relative to experimental crystal structures.

**Comparison to Crystal Structures and the Motion of the Counterion Cluster During the Photoreaction.** The Wat402 counterion has long been an item of interest in the function of bR as the component of the Schiff base counterion cluster that is in direct contact with the Schiff base nitrogen, $N_Z$, of RPSB.[78−80] A recent time-resolved X-ray crystallography experiment[32] emphasized the movement of Wat402 away from $N_Z$ shortly following photoexcitation and cleavage of the hydrogen bond between Wat402 and the Schiff base as key steps in bR photoisomerization. We find this movement to be much less pronounced and suggest that hydrogen bond cleavage is not at all necessary. As discussed below, this suggestion is indeed supported by the latest experiment[33] (which appeared as this paper was being finalized). This is particularly salient in the context of bacterial rhodopsins in general, whose functions, including at the femtosecond time scale, are heavily modulated by the counterion(s) to the RPSB Schiff base.[8] For bR, the observations regarding the dynamic evolution of the counterion cluster can be compared to details provided by experimentally obtained crystal structures.

We find excellent agreement in the Franck−Condon region and in the fluorescent region between the 2018 crystal structures[32] and our simulations, as depicted in Figure 7a and b. Here, the configuration of RPSB and its counterions are averaged over all 30 AIMS simulations in the Franck−Condon region and in the fluorescent region to approximate the experimental crystal structures for the excited ground state, bR*, and I fluorescent state. The RPSB and the Asp85 and Asp212 residues of the counterion cluster are well-aligned and the structural waters occupy the same space within experimental uncertainty. In the Franck−Condon region (Figure 7a), Wat402 lies 2.49 ± 0.06 Å away from $N_Z$ on average. By the time the excited state wavepacket enters the fluorescent region, taken to be in the 49−406 fs time window to match the 6G7I crystal structure, this average distance increases to 2.57 ± 0.05 Å (Figure 7b). The weakening of the hydrogen bond, as reported experimentally, is reflected in our simulations, as observed in Figure 7d, which demonstrates the elongation of the Wat402−$N_Z$ distance almost immediately following photoexcitation.

There is, however, a discrepancy in the average displacement of the counterion cluster, which is most easily visible in the J state (Figure 7c). The J structure from simulation is obtained by averaging over all AIMS simulations in the 457−646 fs time window, corresponding to the experimental 6G7J crystal structure. RPSB and the Asp212 residue remain in good agreement with the experimental crystal structure, but theory and experiment disagree on the displacement of the three waters and the Asp85 residue in the counterion cluster. In experiment, there is a large displacement of Wat402, measuring 3.65 Å and a compensating displacement of Asp85 in the same direction. Meanwhile, in our simulations, there is almost no change in the displacement of the counterion cluster, with the average Wat402−$N_Z$ distance measuring 2.56 ± 0.19 Å in this time window. However, as indicated by the increase in the standard error of this measurement to 0.19 Å, there is significant variance in the Wat402−$N_Z$ distance among each of the 30 AIMS simulations. The increase in the Wat402−$N_Z$ distance that accompanies photoisomerization to the J state can be more easily observed by selecting only TBFs that result in the isomerized photoproduct. This is shown in Figure 7e, where the evolution of the Wat402−$N_Z$ distance is marked as a


DOI: 10.1021/jacs.9b08941
J. Am. Chem. Soc. 2019, 141, 18193−18203

solid blue line for the J photoproduct and as a dashed blue line for the recovered bR ground state following internal conversion and the branching of the photoproducts. There is a significant increase in the Wat402−$N_Z$ distance to over 2.7 Å when RPSB isomerizes, although this shift is smaller than that observed in the 6G7J crystal structure. Even more recently, a second time-resolved serial femtosecond crystallography experiment, published while this article was being completed, has argued in favor of smaller magnitude changes in the Wat402−$N_Z$ distance, citing an increase in the Wat402−$N_Z$ distance to 3.08 Å instead of 3.65 Å by the time J is formed.[33] The elongation and then recovery in the Wat402−$N_Z$ distance as bR proceeds from the conical intersection to the J state, as depicted in Figure 7e, is also reflected in this 2019 experimental study. The predictions we have made here in our theoretical study of the dynamics of RPSB in bR are thus in excellent agreement with findings reported in the near-simultaneous and completely independent experimental work.

In our simulations, the complete deterioration of the hydrogen bond between the RPSB Schiff base and Wat402 is not required for the completion of the RPSB photoisomerization. This contrasts with the 2018 experimental crystal structures that show that a broken hydrogen bond by the time the J state has formed. However, observations in our simulations and in a very recent experimental study[33] suggest that the large-scale movement of the counterions and Wat402 may not be an absolute necessity. The internal conversion from the excited state to the ground state occurs on a time scale and with a branching ratio consistent with previous experimental measurements, and the fluorescence spectrum from our excited state dynamics is consistent with that reported experimentally. Moreover, the structural evolution of RPSB in time on the excited state and the ground state, as shown in Figure 7a−c, reflect good validation of our dynamics results relative to experimental results. The discrepancy between experiment and theory in the displacement of Wat402 thus suggests that the weakened, although unbroken, hydrogen bond may suffice to allow the RPSB photoisomerization to proceed to completion without any significant effect on the speed, efficiency or specificity of the ultrafast photoreaction.

## CONCLUSIONS

Here, we have simulated the nonadiabatic dynamics of RPSB in bR to provide insight into three outstanding questions regarding the photodynamics in the ultrafast photoisomerization reaction: the characterization of the I fluorescent state, the time scales associated with stages of the excited state evolution, and the necessity of the Wat402−$N_Z$ hydrogen bond breakage during photoisomerization. Our simulations are well-validated, having produced an excited state lifetime of 692 ± 221 fs (experimental values: 500−900 fs[13,26,28,29,31]), a quantum yield of 0.65 for the isomerized 13-*cis* photoproduct (experimental values: 0.6−0.7[14,15]), fluorescence spectra in close agreement with experimental measurements, and good structural overlap with experimental crystal structures. We have elucidated three distinct stages for the excited state evolution of RPSB in bR following photoexcitation: (1) relaxation of the RPSB in the bond length alternation coordinate, (2) dwell time in the fluorescent state, and (3) fast torsional motion to the conical intersection. Furthermore, we have provided characterization for the I fluorescent state as featuring an untwisted, bond length inverted RPSB, which is separated from the conical intersection by a small barrier of 3.4 kcal $mol^{-1}$ on the excited state. Lastly, we have presented evidence that the photoreaction is unhindered by the unbroken Wat402−$N_Z$ hydrogen bond, a predictive result from theory that is consistent with recent experimental work published after the completion of our own study. Thus, we have provided insight into three key deficiencies in the current understanding of the ultrafast photoreaction in bR. Outstanding questions remain regarding the catalysis of the photoreaction by the protein environment, specifically as to the roles of the immediate chromophore pocket and the electric field induced by the protein, and structural changes, especially in more remote residues, associated with movements in the Schiff base counterion complex. These are natural future directions for continued research on bR.

## ASSOCIATED CONTENT

### Supporting Information

The Supporting Information is available free of charge on the ACS Publications website at DOI: 10.1021/jacs.9b08941.

Figure for the reduced QM/MM subsystem used in AIMD and AIMS simulations, plot of the excited state population decay for individual AIMS simulations, plot of the steady state fluorescence, zoomed-in 2D fluorescence plot demonstrating wavelength-dependent behavior, minimum energy path comparison between the full and reduced QM regions, plot of averaged RPSB BLA in time, plot of population transfer specificity, plot of averaged RPSB torsion in time (PDF)

Further details for crystal structure comparisons (ZIP)

## AUTHOR INFORMATION


### Corresponding Author

*todd.martinez@stanford.edu

### ORCID

Ruibin Liang: 0000-0001-8741-1520

Fang Liu: 0000-0003-1322-4997

Todd J. Martínez: 0000-0002-4798-8947


### Notes

The authors declare no competing financial interest.

## ACKNOWLEDGMENTS

This work was supported by the Center for Quantum Molecular Design (CQMD) through the National Science Foundation (CHE-1740645). Computational support was provided through the AMOS program within the Chemical Sciences, Geosciences and Biosciences Division of the Office of Basic Energy Sciences, Office of Science, U.S. Department of Energy.

## REFERENCES


(1) Oesterhelt, D.; Stoeckenius, W. Rhodopsin-like Protein from the Purple Membrane of Halobacterium halobium. *Nat. New Biol.* **1971**, *233*, 149.

(2) Spudich, J. L.; Bogomolni, R. A. Mechanism of colour discrimination by a bacterial sensory rhodopsin. *Nature* **1984**, *312*, 509.

(3) Jung, K.-H.; Trivedi, V. D.; Spudich, J. L. Demonstration of a sensory rhodopsin in eubacteria. *Mol. Microbiol.* **2003**, *47*, 1513.

(4) Miesenböck, G. Optogenetic Control of Cells and Circuits. *Annu. Rev. Cell Dev. Biol.* **2011**, *27*, 731.




DOI: 10.1021/jacs.9b08941
J. Am. Chem. Soc. 2019, 141, 18193−18203

(5) Racker, E.; Stoeckenius, W. Reconstitution of Purple Membrane Vesicles Catalyzing Light-driven Proton Uptake and Adenosine Triphosphate Formation. *J. Biol. Chem.* **1974**, *249*, 662.
(6) Matsuno-Yagi, A.; Mukohata, Y. Two possible roles of bacteriorhodopsin; a comparative study of strains of Halobacterium halobium differing in pigmentation. *Biochem. Biophys. Res. Commun.* **1977**, *78*, 237.
(7) Pebay-Peyroula, E.; Rummel, G.; Rosenbusch, J. P.; Landau, E. M. X-ray Structure of Bacteriorhodopsin at 2.5 Angstroms from Microcrystals Grown in Lipidic Cubic Phases. *Science* **1997**, *277*, 1676.
(8) Ernst, O. P.; Lodowski, D. T.; Elstner, M.; Hegemann, P.; Brown, L. S.; Kandori, H. Microbial and Animal Rhodopsins: Structures, Functions, and Molecular Mechanisms. *Chem. Rev.* **2014**, *114*, 126.
(9) Gozem, S.; Luk, H. L.; Schapiro, I.; Olivucci, M. Theory and Simulation of the Ultrafast Double-Bond Isomerization of Biological Chromophores. *Chem. Rev.* **2017**, *117*, 13502.
(10) Logunov, S. L.; Song, L.; El-Sayed, M. A. Excited-State Dynamics of a Protonated Retinal Schiff Base in Solution. *J. Phys. Chem.* **1996**, *100*, 18586.
(11) Punwong, C.; Owens, J.; Martínez, T. J. Direct QM/MM Excited-State Dynamics of Retinal Protonated Schiff Base in Isolation and Methanol Solution. *J. Phys. Chem. B* **2015**, *119*, 704.
(12) Dobler, J.; Zinth, W.; Kaiser, W.; Oesterhelt, D. Excited-state reaction dynamics of bacteriorhodopsin studied by femtosecond spectroscopy. *Chem. Phys. Lett.* **1988**, *144*, 215.
(13) Mathies, R. A.; Brito Cruz, C. H.; Pollard, W. T.; Shank, C. V. Direct observation of the femtosecond excited-state cis-trans isomerization in bacteriorhodopsin. *Science* **1988**, *240*, 777.
(14) Tittor, J.; Oesterhelt, D. The quantum yield of bacteriorhodopsin. *FEBS Lett.* **1990**, *263*, 269.
(15) Govindjee, R.; Balashov, S. P.; Ebrey, T. G. Quantum efficiency of the photochemical cycle of bacteriorhodopsin. *Biophys. J.* **1990**, *58*, 597.
(16) Smith, S. O.; Lugtenburg, J.; Mathies, R. A. Determination of retinal chromophore structure in bacteriorhodopsin with resonance Raman spectroscopy. *J. Membr. Biol.* **1985**, *85*, 95.
(17) Applebury, M. L.; Peters, K. S.; Rentzepis, P. M. Primary intermediates in the photochemical cycle of bacteriorhodopsin. *Biophys. J.* **1978**, *23*, 375.
(18) Ippen, E. P.; Shank, C. V.; Lewis, A.; Marcus, M. A. Subpicosecond spectroscopy of bacteriorhodopsin. *Science* **1978**, *200*, 1279.
(19) Kaufmann, K. J.; Sundstrom, V.; Yamane, T.; Rentzepis, P. M. Kinetics of the 580-nm ultrafast bacteriorhodopsin transient. *Biophys. J.* **1978**, *22*, 121.
(20) Nuss, M. C.; Zinth, W.; Kaiser, W.; Kölling, E.; Oesterhelt, D. Femtosecond spectroscopy of the first events of the photochemical cycle in bacteriorhodopsin. *Chem. Phys. Lett.* **1985**, *117*, 1.
(21) Sharkov, A. V.; Pakulev, A. V.; Chekalin, S. V.; Matveetz, Y. A. Primary events in bacteriorhodopsin probed by subpicosecond spectroscopy. *Biochim. Biophys. Acta, Bioenerg.* **1985**, *808*, 94.
(22) Zhong, Q.; Ruhman, S.; Ottolenghi, M.; Sheves, M.; Friedman, N.; Atkinson, G. H.; Delaney, J. K. Reexamining the Primary Light-Induced Events in Bacteriorhodopsin Using a Synthetic C-13 = c-14-Locked Chromophore. *J. Am. Chem. Soc.* **1996**, *118*, 12828.
(23) Ye, T.; Friedman, N.; Gat, Y.; Atkinson, G. H.; Sheves, M.; Ottolenghi, M.; Ruhman, S. On the Nature of the Primary Light-Induced Events in Bacteriorhodopsin: Ultrafast Spectroscopy of Native and C13 = C14 Locked Pigments. *J. Phys. Chem. B* **1999**, *103*, 5122.
(24) Haacke, S.; Vinzani, S.; Schenkl, S.; Chergui, M. Spectral and Kinetic Fluorescence Properties of Native and Nonisomerizing Retinal in Bacteriorhodopsin. *ChemPhysChem* **2001**, *2*, 310.
(25) Hasson, K. C.; Gai, F.; Anfinrud, P. A. The Photoisomerization of Retinal in Bacteriorhodopsin: Experimental Evidence for a Three-State Model. *Proc. Natl. Acad. Sci. U. S. A.* **1996**, *93*, 15124.
(26) Gai, F.; Hasson, K. C.; McDonald, J. C.; Anfinrud, P. A. Chemical Dynamics in Proteins: The Photoisomerization of Retinal in Bacteriorhodopsin. *Science* **1998**, *279*, 1886.
(27) Logunov, S. L.; Masciangioli, T. M.; Kamalov, V. F.; El-Sayed, M. A. Low-Temperature Retinal Photoisomerization Dynamics in Bacteriorhodopsin. *J. Phys. Chem. B* **1998**, *102*, 2303.
(28) Kobayashi, T.; Saito, T.; Ohtani, H. Real-time spectroscopy of transition states in bacteriorhodopsin during retinal isomerization. *Nature* **2001**, *414*, 531.
(29) Herbst, J.; Heyne, K.; Diller, R. Femtosecond Infrared Spectroscopy of Bacteriorhodopsin Chromophore Isomerization. *Science* **2002**, *297*, 822.
(30) Kahan, A.; Nahmias, O.; Friedman, N.; Sheves, M.; Ruhman, S. Following Photoinduced Dynamics in Bacteriorhodopsin with 7-fs Impulsive Vibrational Spectroscopy. *J. Am. Chem. Soc.* **2007**, *129*, 537.
(31) Shim, S.; Dasgupta, J.; Mathies, R. A. Femtosecond Time-Resolved Stimulated Raman Reveals the Birth of Bacteriorhodopsin's J and K Intermediates. *J. Am. Chem. Soc.* **2009**, *131*, 7592.
(32) Nogly, P.; Weinert, T.; James, D.; Carbajo, S.; Ozerov, D.; Furrer, A.; Gashi, D.; Borin, V.; Skopintsev, P.; Jaeger, K.; Nass, K.; Båth, P.; Bosman, R.; Koglin, J.; Seaberg, M.; Lane, T.; Kekilli, D.; Brünle, S.; Tanaka, T.; Wu, W.; Milne, C.; White, T.; Barty, A.; Weierstall, U.; Panneels, V.; Nango, E.; Iwata, S.; Hunter, M.; Schapiro, I.; Schertler, G.; Neutze, R.; Standfuss, J. Retinal isomerization in bacteriorhodopsin captured by a femtosecond x-ray laser. *Science* **2018**, *361*, No. eaat0094.
(33) Nass Kovacs, G.; Colletier, J.-P.; Grünbein, M. L.; Yang, Y.; Stensitzki, T.; Batyuk, A.; Carbajo, S.; Doak, R. B.; Ehrenberg, D.; Foucar, L.; Gasper, R.; Gorel, A.; Hilpert, M.; Kloos, M.; Koglin, J. E.; Reinstein, J.; Roome, C. M.; Schlesinger, R.; Seaberg, M.; Shoeman, R. L.; Stricker, M.; Boutet, S.; Haacke, S.; Heberle, J.; Heyne, K.; Domratcheva, T.; Barends, T. R. M.; Schlichting, I. Three-dimensional view of ultrafast dynamics in photoexcited bacteriorhodopsin. *Nat. Commun.* **2019**, *10*, 3177.
(34) Warshel, A.; Chu, Z. T. Nature of the Surface Crossing Process in Bacteriorhodopsin: Computer Simulations of the Quantum Dynamics of the Primary Photochemical Event. *J. Phys. Chem. B* **2001**, *105*, 9857.
(35) Hayashi, S.; Tajkhorshid, E.; Schulten, K. Molecular Dynamics Simulation of Bacteriorhodopsin's Photoisomerization Using Ab Initio Forces for the Excited Chromophore. *Biophys. J.* **2003**, *85*, 1440.
(36) Li, X.; Chung, L. W.; Morokuma, K. Photodynamics of All-trans Retinal Protonated Schiff Base in Bacteriorhodopsin and Methanol Solution. *J. Chem. Theory Comput.* **2011**, *7*, 2694.
(37) Punwong, C.; Martínez, T. J.; Hannongbua, S. Direct QM/MM simulation of photoexcitation dynamics in bacteriorhodopsin and halorhodopsin. *Chem. Phys. Lett.* **2014**, *610–611*, 213.
(38) Du, M.; Fleming, G. R. Femtosecond time-resolved fluorescence spectroscopy of bacteriorhodopsin: Direct observation of excited state dynamics in the primary step of the proton pump cycle. *Biophys. Chem.* **1993**, *48*, 101.
(39) Schenkl, S.; Portuondo, E.; Zgrablić, G.; Chergui, M.; Haacke, S.; Friedman, N.; Sheves, M. Ultrafast energy relaxation in bacteriorhodopsin studied by time-integrated fluorescence. *Phys. Chem. Chem. Phys.* **2002**, *4*, 5020.
(40) Ruhman, S.; Hou, B.; Friedman, N.; Ottolenghi, M.; Sheves, M. Following Evolution of Bacteriorhodopsin in Its Reactive Excited State via Stimulated Emission Pumping. *J. Am. Chem. Soc.* **2002**, *124*, 8854.
(41) Schmidt, B.; Sobotta, C.; Heinz, B.; Laimgruber, S.; Braun, M.; Gilch, P. Excited-state dynamics of bacteriorhodopsin probed by broadband femtosecond fluorescence spectroscopy. *Biochim. Biophys. Acta, Bioenerg.* **2005**, *1706*, 165.
(42) Garavelli, M.; Vreven, T.; Celani, P.; Bernardi, F.; Robb, M. A.; Olivucci, M. Photoisomerization Path for a Realistic Retinal Chromophore Model: The Nonatetraeniminium Cation. *J. Am. Chem. Soc.* **1998**, *120*, 1285.
(43) Altoè, P.; Cembran, A.; Olivucci, M.; Garavelli, M. Aborted double bicycle-pedal isomerization with hydrogen bond breaking is


DOI: 10.1021/jacs.9b08941
*J. Am. Chem. Soc.* 2019, 141, 18193−18203

the primary event of bacteriorhodopsin proton pumping. *Proc. Natl. Acad. Sci. U. S. A.* **2010**, *107*, 20172.
(44) Liang, R.; Liu, F.; Martínez, T. J. Nonadiabatic Photodynamics of Retinal Protonated Schiff Base in Channelrhodopsin 2. *J. Phys. Chem. Lett.* **2019**, *10*, 2862.
(45) Jo, S.; Kim, T.; Iyer, V. G.; Im, W. CHARMM-GUI: A web-based graphical user interface for CHARMM. *J. Comput. Chem.* **2008**, *29*, 1859.
(46) Wu, E. L.; Cheng, X.; Jo, S.; Rui, H.; Song, K. C.; Dávila-Contreras, E. M.; Qi, Y.; Lee, J.; Monje-Galvan, V.; Venable, R. M.; Klauda, J. B.; Im, W. CHARMM-GUI Membrane Builder toward realistic biological membrane simulations. *J. Comput. Chem.* **2014**, *35*, 1997.
(47) Wang, J.; Wolf, R. M.; Caldwell, J. W.; Kollman, P. A.; Case, D. A. Development and testing of a general amber force field. *J. Comput. Chem.* **2004**, *25*, 1157.
(48) Wang, J.; Wang, W.; Kollman, P. A.; Case, D. A. Automatic atom type and bond type perception in molecular mechanical calculations. *J. Mol. Graphics Modell.* **2006**, *25*, 247.
(49) Maier, J. A.; Martinez, C.; Kasavajhala, K.; Wickstrom, L.; Hauser, K. E.; Simmerling, C. ff14SB: Improving the Accuracy of Protein Side Chain and Backbone Parameters from ff99SB. *J. Chem. Theory Comput.* **2015**, *11*, 3696.
(50) Dickson, C. J.; Madej, B. D.; Skjevik, Å. A.; Betz, R. M.; Teigen, K.; Gould, I. R.; Walker, R. C. Lipid14: The Amber Lipid Force Field. *J. Chem. Theory Comput.* **2014**, *10*, 865.
(51) Wu, Y.; Tepper, H. L.; Voth, G. A. Flexible simple point-charge water model with improved liquid-state properties. *J. Chem. Phys.* **2006**, *124*, 024503.
(52) Sasaki, J.; Lanyi, J. K.; Needleman, R.; Yoshizawa, T.; Maeda, A. Complete identification of C = O stretching vibrational bands of protonated aspartic acid residues in the difference infrared spectra of M and N intermediates versus bacteriorhodopsin. *Biochemistry* **1994**, *33*, 3178.
(53) Brown, L. S.; Varo, G.; Hatanaka, M.; Sasaki, J.; Kandori, H.; Maeda, A.; Friedman, N.; Sheves, M.; Needleman, R.; Lanyi, J. K. The complex extracellular domain regulates the deprotonation and reprotonation of the retinal Schiff base during the bacteriorhodopsin photocycle. *Biochemistry* **1995**, *34*, 12903.
(54) Eastman, P.; Swails, J.; Chodera, J. D.; McGibbon, R. T.; Zhao, Y.; Beauchamp, K. A.; Wang, L.-P.; Simmonett, A. C.; Harrigan, M. P.; Stern, C. D.; Wiewiora, R. P.; Brooks, B. R.; Pande, V. S. OpenMM 7: Rapid development of high performance algorithms for molecular dynamics. *PLoS Comput. Biol.* **2017**, *13*, No. e1005659.
(55) Leimkuhler, B.; Matthews, C. In *Molecular Dynamics with Deterministic and Stochastic Numerical Methods*; Springer: 2015.
(56) Ufimtsev, I. S.; Martinez, T. J. Quantum Chemistry on Graphical Processing Units. 3. Analytical Energy Gradients, Geometry Optimization, and First Principles Molecular Dynamics. *J. Chem. Theory Comput.* **2009**, *5*, 2619.
(57) Bussi, G.; Parrinello, M. Accurate sampling using Langevin dynamics. *Phys. Rev. E* **2007**, *75*, 056707.
(58) Ufimtsev, I. S.; Martínez, T. J. Quantum Chemistry on Graphical Processing Units. 1. Strategies for Two-Electron Integral Evaluation. *J. Chem. Theory Comput.* **2008**, *4*, 222.
(59) Ufimtsev, I. S.; Martinez, T. J. Quantum Chemistry on Graphical Processing Units. 2. Direct Self-Consistent-Field Implementation. *J. Chem. Theory Comput.* **2009**, *5*, 1004.
(60) Rohrdanz, M. A.; Martins, K. M.; Herbert, J. M. A long-range-corrected density functional that performs well for both ground-state properties and time-dependent density functional theory excitation energies, including charge-transfer excited states. *J. Chem. Phys.* **2009**, *130*, 054112.
(61) Filatov, M.; Liu, F.; Kim, K. S.; Martínez, T. J. Self-consistent implementation of ensemble density functional theory method for multiple strongly correlated electron pairs. *J. Chem. Phys.* **2016**, *145*, 244104.
(62) Filatov, M.; Liu, F.; Martínez, T. J. Analytical derivatives of the individual state energies in ensemble density functional theory method. I. General formalism. *J. Chem. Phys.* **2017**, *147*, 034113.
(63) Liu, F.; Filatov, M.; Martínez, T. J. Analytical Derivatives of the Individual State Energies in Ensemble Density Functional Theory Method: II. Implementation on Graphical Processing Units (GPUs). *ChemRxiv* **2019**, DOI: 10.26434/chemrxiv.7985657.v1.
(64) Roos, B. O. *In Advances in Chemical Physics* **2007**, *69*, 399.
(65) Levine, B. G.; Ko, C.; Quenneville, J.; Martinez, T. J. Conical intersections and double excitations in time-dependent density functional theory. *Mol. Phys.* **2006**, *104*, 1039.
(66) Nikiforov, A.; Gamez, J. A.; Thiel, W.; Huix-Rotllant, M.; Filatov, M. Assessment of approximate computational methods for conical intersections and branching plane vectors in organic molecules. *J. Chem. Phys.* **2014**, *141*, 124122.
(67) Gozem, S.; Melaccio, F.; Valentini, A.; Filatov, M.; Huix-Rotllant, M.; Ferre, N.; Frutos, L. M.; Angeli, C.; Krylov, A. I.; Granovsky, A. A.; Lindh, R.; Olivucci, M. Shape of Multireference, Equation-Of-Motion Coupled Cluster, and Density Functional Theory Potential Energy Surfaces at a Conical Intersection. *J. Chem. Theory Comput.* **2014**, *10*, 3074.
(68) Liu, L.; Liu, J.; Martinez, T. J. Dynamical Correlation Effects on Photoisomerization: Ab Initio Multiple Spawning Dynamics with MS-CASPT2 for a Model trans-Protonated Schiff Base. *J. Phys. Chem. B* **2016**, *120*, 1940.
(69) Ben-Nun, M.; Martínez, T. J. Nonadiabatic molecular dynamics: Validation of the multiple spawning method for a multidimensional problem. *J. Chem. Phys.* **1998**, *108*, 7244.
(70) Ben-Nun, M.; Quenneville, J.; Martínez, T. J. Ab Initio Multiple Spawning: Photochemistry from First Principles Quantum Molecular Dynamics. *J. Phys. Chem. A* **2000**, *104*, 5161.
(71) Ben-Nun, M.; Molnar, F.; Schulten, K.; Martínez, T. J. The role of intersection topography in bond selectivity of cis-trans photoisomerization. *Proc. Natl. Acad. Sci. U. S. A.* **2002**, *99*, 1769.
(72) Crespo-Otero, R.; Barbatti, M. Recent advances and perspectives on nonadiabatic mixed quantum-classical dynamics. *Chem. Rev.* **2018**, *118*, 7026.
(73) Curchod, B. F. E.; Martinez, T. J. Ab Initio Nonadiabatic Quantum Molecular Dynamics. *Chem. Rev.* **2018**, *118*, 3305.
(74) Tully, J. C. Molecular dynamics with electronic transitions. *J. Chem. Phys.* **1990**, *93*, 1061.
(75) McGibbon, R. T.; Beauchamp, K. A.; Harrigan, M. P.; Klein, C.; Swails, J. M.; Hernandez, C. X.; Schwantes, C. R.; Wang, L.-P.; Lane, T. J.; Pande, V. S. MDTraj: A Modern Open Library for the Analysis of Molecular Dynamics Trajectories. *Biophys. J.* **2015**, *109*, 1528.
(76) Briand, J.; Léonard, J.; Haacke, S. Ultrafast photo-induced reaction dynamics in bacteriorhodopsin and its Trp mutants. *J. Opt.* **2010**, *12*, 084004.
(77) Kiefer, H. V.; Gruber, E.; Langeland, J.; Kusochek, P. A.; Bochenkova, A. V.; Andersen, L. H. Intrinsic photoisomerization dynamics of protonated Schiff-base retinal. *Nat. Commun.* **2019**, *10*, 1210.
(78) Luecke, H.; Schobert, B.; Richter, H.-T.; Cartailler, J.-P.; Lanyi, J. K. Structure of bacteriorhodopsin at 1.55 Å resolution. *J. Mol. Biol.* **1999**, *291*, 899.
(79) Hayashi, S.; Ohmine, I. Proton Transfer in Bacteriorhodopsin: Structure, Excitation, IR Spectra, and Potential Energy Surface Analyses by an ab Initio QM/MM Method. *J. Phys. Chem. B* **2000**, *104*, 10678.
(80) Shibata, M.; Tanimoto, T.; Kandori, H. Water Molecules in the Schiff Base Region of Bacteriorhodopsin. *J. Am. Chem. Soc.* **2003**, *125*, 13312.


DOI: 10.1021/jacs.9b08941
*J. Am. Chem. Soc.* 2019, 141, 18193−18203